RSC Advances

ROYAL SOCIETY OF CHEMISTRY

www.rsc.org/advances

Facile fabrication of mpg-C_3N_4/TiO_2 heterojunction photocatalyst with enhanced visible light photoactivity toward organic pollutant degradation

Shuaishuai Ma,‡ Jinjuan Xue,‡ Yuming Zhou,* Zewu Zhang, Zhilan Cai, Daibao Zhu, Shuang Liang

School of Chemistry and Chemical Engineering, Southeast University, Nanjing 211189, P. R. China

Abstract A facile hard template approach has been developed to prepare mpg-C_3N_4/TiO_2 composites using SiO_2 nanoparticles as hard template and cyanamide as precursor. The samples were well characterized by X-ray diffraction (XRD), energy-dispersive X-ray spectroscopy (EDS), transmission electron microscopy (TEM), and ultraviolet-visible diffuse reflectance spectroscopy (UV-vis DRS). The results demonstrated that TiO_2 nanoparticles sized 5-10 nm were distributed on the surface of mpg-C_3N_4 to form the mpg-C_3N_4/TiO_2 heterojunction photocatalyst. In this way, the mpg-C_3N_4/TiO_2 heterojunction catalysts have a porous structure and large surface areas, which increase the contact area of pollutants. Rhodamine B (RhB) was carried out as a representative organic pollutant to evaluate the photocatalytic activity of samples under visible light irradiation. The results showed that the as-prepared mpg-C_3N_4/TiO_2 heterojunction catalysts significantly enhanced the visible photocatalytic activity compared to pure mpg-C_3N_4 and the degradation rate was 1.6 times higher than that of pure mpg-C_3N_4. The increased photocatalytic activity of mpg-C_3N_4/TiO_2 heterojunction can be attributed to the formation of the heterojunction between mpg-C_3N_4 and TiO_2, which suppresses the recombination of photoinduced electron-hole pairs. Furthermore, based on systematic characterizations and discussions, a possible photocatalytic mechanism for the excellent

* Corresponding author. Tel.: +86 25 52090617; fax: +86 25 52090617.
E-mail address: ymzhou@seu.edu.cn (Yuming Zhou).
‡S.S. Ma and J.J. Xue contributed equally to this work.

photocatalytic performance was proposed.

Introduction

In decades, environmental problems such as organic pollutants and toxic water pollutants produced by some industries have become more and more harmful to human health.[1-3] Photocatalysis is highly expected to be a green technology for solving many current environmental and energy issues through its efficiency and broad applicability.[4] With the steady and fast growing field of nanoscience and nanotechnology, various nanostructured semiconductor materials such as metal oxides, nitrides and sulfides have been exploited as photocatalysts for photocatalytic degradation of organic pollutants.[5] Notably, TiO_2 is widely studied due to its favorable optical and electronic properties, long-term stability, low cost, and nontoxicity. However, with a bandgap of 3.2 eV, TiO_2 could only utilize radiation with wavelength less than 390 nm, which only takes 5% of the solar light. The narrow optical absorption range and the high efficiency recombination of photogenerated electrons and holes are the main factors answering for low energy efficiency.[6] Therefore, lots of efforts have been devoted to extend the absorption edge of TiO_2, such as doping of TiO_2 with metallic or nonmetallic elements to increase the visible light absorbance,[7-9] and coupling with other semiconductors to increase the separation efficiency of photogenerated electron-hole pairs during photocatalysis.[10, 11] Considering that most light sources include plenty of visible light, coupling a wide-bandgap semiconductor with small-bandgap inorganic semiconductor as visible light sensitizer is a key issue for enhancing photocatalytic energy efficiency to develop new photocatalysts with good photogenerated charge separation as well as wide response wavelength range.

Recently, graphitic carbon nitride (g-C_3N_4), a polymeric metal-free semiconductor with a band gap of about 2.70 eV, has been recently focused on the photocatalytic field such as water splitting and/or organic pollutant decomposition owing to its unique two-dimensional structure, excellent chemical stability and tunable electronic structure.[12-14] However, the photocatalytic efficiency of g-C_3N_4 is still limited due to the high recombination rate of photogenerated

electron-hole pairs. Several methods have been developed to improve the photocatalytic performance of g-C_3N_4, for instance, dye sensitization, transition metal doping and coupled semiconductor.[15-20] Specially, g-C_3N_4 have the highest occupied molecular orbital (HOMO) which located at -1.12 eV and is more negative than the conduction band (CB) of the common wide bandgap semiconductor photocatalysts such as ZnO and TiO_2, which is favorable to form heterojunctions with the wide bandgap semiconductors and thus to extend their visible light response.[21] In particular, the fabrication of heterostructured composites by combining g-C_3N_4 with other semiconductors can not only restrict efficiently the recombination of photogenerated charge carriers, but also endow the composites novel characteristics or some enhanced properties by the synergistic effects or antagonistic effects.[22, 23] In addition, the previous works indicated that porous structure introduced in g-C_3N_4 by soft or hard templates would make it possess increased surface area and provide more active sites for adsorption and photocatalytic reaction, which are also beneficial to the enhancement of photocatalytic efficiency.[24-26]

In this paper, we demonstrated a facile hard template method to synthesize mpg-C_3N_4/TiO_2 heterostructures. Herein, mesoporous g-C_3N_4 (mpg-C_3N_4) with an open crystalline pore wall and a large surface area was used as a support to disperse TiO_2 nanoparticles. The mesoporous structure can in principle enhance the light harvesting ability and the reactant adsorption capability of the material due to its large surface area and multiple scattering effects. The photocatalytic activity of the mpg-C_3N_4/TiO_2 heterostructures was carefully investigated by degradation of Rhodamine B (RhB) dye under visible light irradiation. The results indicated that the as-prepared mpg-C_3N_4/TiO_2 heterostructures exhibit much higher visible photocatalytic activity than that of bare mpg-C_3N_4 and TiO_2 nanoparticles, which is attributed to the improvement in the separation efficiency of photogenerated electron-hole pairs in mpg-C_3N_4/TiO_2 composites. Meanwhile, we also proposed a possible mechanism for the enhanced activity of mpg-C_3N_4/TiO_2 composites on account of the experimental results.

Experimental section

Materials

Cyanamide ($CN-NH_2$, 50%), 40% dispersion of SiO_2 particles (12 nm, Ludox HS40), titanium oxide (TiO_2, 5-10 nm) and ammonium bifluoride (NH_4HF_2) were purchased from Aladdin Chemical Regent Co., Ltd. (Shanghai, China). All the reagents in this experiment are analytically pure and used without further purification.

Preparation of mpg-C_3N_4/TiO_2 heterostructures

In a typical procedure, 8.0 g of cyanamide (50% solution) was added dropwise to 24 g 40% dispersion of 12 nm SiO_2 particles, which were used as a hard template, and then 0.5 g TiO_2 powder was added in the above solution with ultrasonication. The mixture was heated at 80 °C with stirring to evaporate water. The resulting white powder was then heated at a rate of 2.3 °C min^{-1} over 4 h to reach a temperature of 550 °C, and then keep at this temperature for another 4 h. The brown-yellow product was treated with a 4 M NH_4HF_2 for two days to remove the silica template. The powder was then centrifuged and washed with distilled and ethanol for several times. Finally the mpg-C_3N_4/TiO_2 was dried at 70 °C under vacuum overnight. Meanwhile, pure mpg-C_3N_4 sample was synthesis without addition of TiO_2 according to the previous report. [27]

Sample characterizations

X-ray diffraction (XRD) patterns were recorded on an X-ray diffractometer (SmartLab, Rigaku) using Cu Ka radiation in the angle range of 10-80° (2θ). Then energy dispersed spectrum (EDS) was used to analyze the element of the as-prepared samples. The FT-IR spectra (KBrdisc) of the as-prepared samples were recorded on a BRUKER-ALPHA FT-IR spectrometer. Transmission electron microscopy (TEM) and high resolution TEM (HRTEM) images were taken with a JEM-2100 high-resolution transmission electron microscope. X-ray photoelectron spectroscopy (XPS) measurement was performed with a Kratos Axis Ultra DLD spectrometer equipped with a monochromatic Al Kα X-ray source (1486.6 eV). The nitrogen adsorption and desorption isotherms were measured at 77 K on an ASAP 2020 (Micromertics USA). UV-vis diffuse reflection spectra (UV-vis DRS) were recorded on UV-vis spectrometer (UV-3650,

Shimadzu) with an integrating sphere attachment. Here, $BaSO_4$ was used as the reflectance standard material. The PL spectra were measured at room temperature on a Shimadzu RF-5301 fluorescence spectrophotometer with 325 nm excitation wavelength.

Photocatalytic activity test

The photocatalytic reaction was carried out at room temperature in a Pyrex reactor with reflux water to keep its temperature constant. A 500 W Xe lamp (Philips) was used as the simulated solar light source (UV-visible light), and a 420 nm cutoff filter was mounted on the lamp to eliminate infrared irradiation. Rhodamine B (RhB) with a concentration of 10 mg L^{-1} was used as the contaminant. In order to obtain an optimally dispersed system and reach complete adsorption-desorption equilibration, 100 mg photocatalyst powder was dispersed in 100 mL reaction solution by ultrasonicating for 10 min, and then the suspension was magnetically stirred in the dark for 1 h. Subsequently, the above suspension was irradiated by the 500 W xenon lamp. At regular intervals, an 3 mL portion of the suspension was sampled and filtered through a 0.45 μm PTFE syringe filter to get clear liquid. The quantitative determination of RhB in the supernatant was then monitored by measuring its intensity of the absorption peak at 553 nm with a UV-vis spectrophotometer (UV-3600; Shimadzu).

Results and discussion

Structure and Morphology

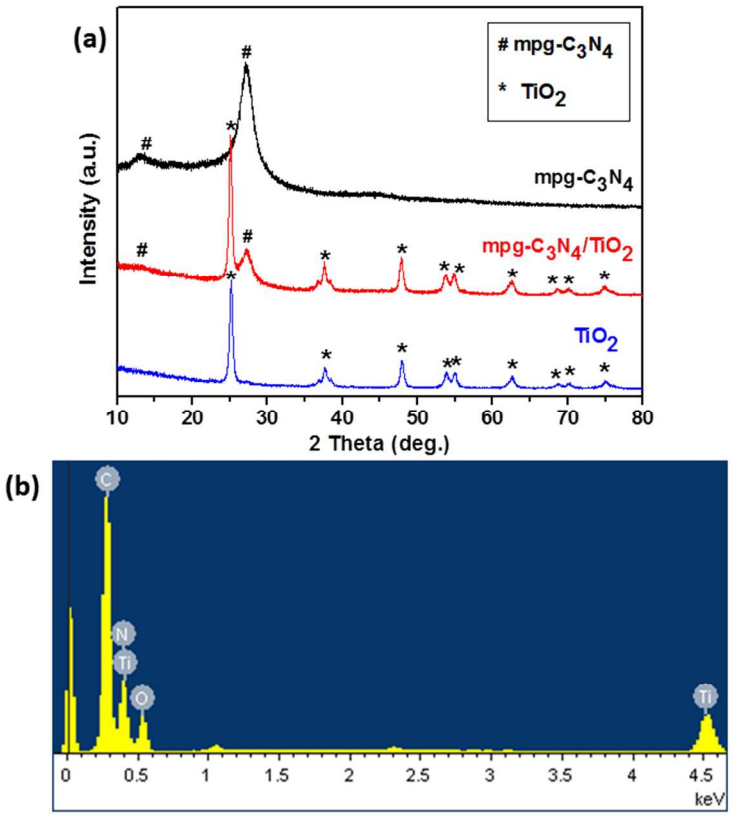

Fig. 1 XRD patterns of (a) mpg-C_3N_4, TiO_2 and mpg-C_3N_4/TiO_2 heterojunctions, and EDS spectrum of (b) the mpg-C_3N_4/TiO_2.

Fig. 1 shows the XRD patterns of the bare mpg-C_3N_4, TiO_2 and mpg-C_3N_4/TiO_2 heterojunctions. As can be seen, the bare mpg-C_3N_4 shows two pronounced diffraction peaks of (100) and (002) planes at $2\theta \approx 13.1^{o}$ and 27.2^{o}, which can be ascribed to the characteristic inter-layer structural packing and the interplanar stacking peaks of the aromatic systems, respectively.[28] In pure TiO_2 sample, the strong diffraction angles at $2\theta = 25.34^{\circ}$, 37.82°, 48.08°, 53.94°, 55.10°, $62.78^{\circ}$and 68.80°, can be assigned to (101), (004), (200), (105), (211), (204) and (116) crystal planes of pure TiO_2 with the anatase phase (JCPDS 21-1272), respectively.[29] The mpg-C_3N_4/TiO_2 heterojunctions sample samples exhibit diffraction peaks corresponding to both mpg-C3N4 and TiO_2, reflecting the presence of two phases, and no other impurity peaks were observed. In addition, EDS analysis was employed to investigate the composition of the heterojunctions (in Fig. 1(b)), where the appeared peaks confirm that the product was only

composed of C, N, O and Ti elements.

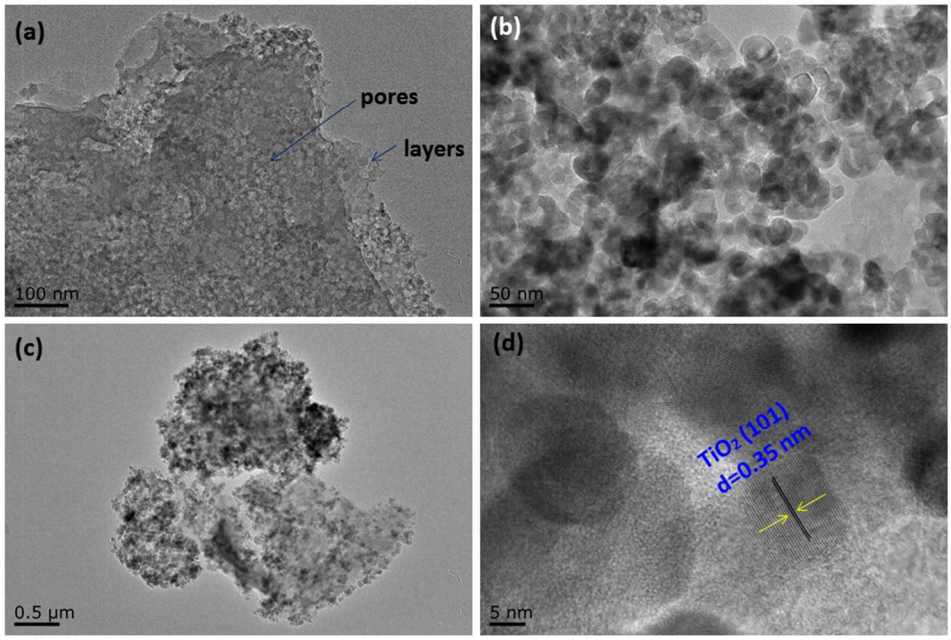

Fig.2 Typical TEM images of (a) mpg-C_3N_4, (b) pure TiO_2, (c) mpg-C_3N_4/TiO_2 heterojunctions and HRTEM (d) image of the as-prepared mpg-C_3N_4/TiO_2 heterojunctions

The morphologies of mpg-C_3N_4, pure TiO_2 and mpg-C_3N_4/TiO_2 heterojunctions were investigated by transmission electron microscopy (TEM) and high resolution TEM (HRTEM), as shown in Fig. 2. As shown in Fig. 2a, mpg-C_3N_4 displays 2D lamellar structure and many spherical pores with a mean diameter of about 12 nm are observed on the surface. These pores exactly reflect the geometric properties of the original template of SiO_2 particles with a mean diameter of 12 nm. Fig. 2b displays the irregular spheres of TiO_2 particles with diameters in the range of 5-10 nm. For the mpg-C_3N_4/TiO_2 heterojunctions (Fig. 2c), the TiO_2 nanoparticles are found embedded in the mpg-C_3N_4 lamellar structure. And the corresponding HRTEM image which shown in Fig. 2d clearly reveals the close interfacial connections between mpg-C_3N_4 and TiO_2 nanoparticles. By measuring the lattice fringes in HRTEM image, the resolved interplanar distance of 0.35 nm, agrees well with the lattice spacing of the (101) plane of anatase TiO_2. These observations suggest the formation of heterojunction between TiO_2 and mpg-C_3N_4 which would be an ideal system to achieve the improved electron-hole separation via smooth charge transfer

process.

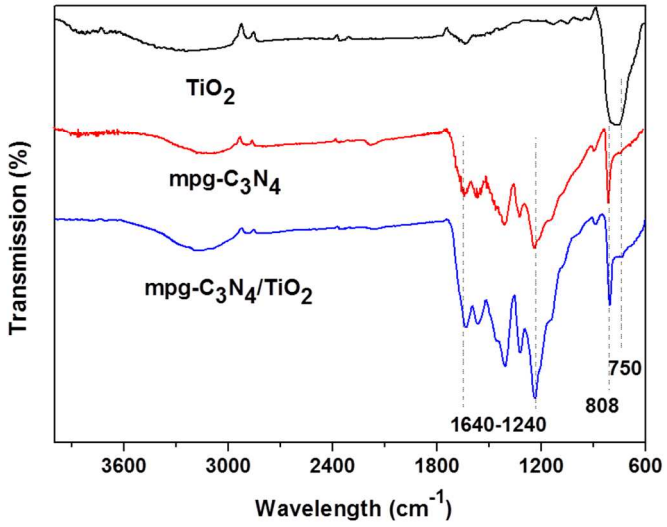

Fig. 3 FTIR spectra of the as-prepared mpg-C_3N_4, TiO_2 and mpg-C_3N_4/TiO_2 heterojunctions.

In order to investigate the interaction between TiO_2 and mpg-C_3N_4 in the as-prepared mpg-C_3N_4/TiO_2 heterojunctions, FTIR spectra were present in Fig. 3. Pure mpg-C_3N_4 shows characteristic IR peaks similar to those of the previous results.[18, 30] The broad peak at 3000-3600 cm^{-1} is contributed by the N-H stretching;[31] the strong band at 1240-1640 cm^{-1} is attributed to the typical stretching vibration of the C-N and C@N heterocycles;[32, 33] and the band near 808 cm^{-1} can be attributed to the characteristic breathing mode of triazine units.[34] It can be seen that a band around 500-700 cm^{-1} is clearly shown in the FTIR spectrum of TiO_2, which corresponds to the Ti-O-Ti stretching vibration.[35] The major characteristic peaks of TiO_2 and mpg-C_3N_4 almost appear in mpg-C_3N_4/TiO_2 sample, further indicating the formation of mpg-C_3N_4/TiO_2 heterojunctions.

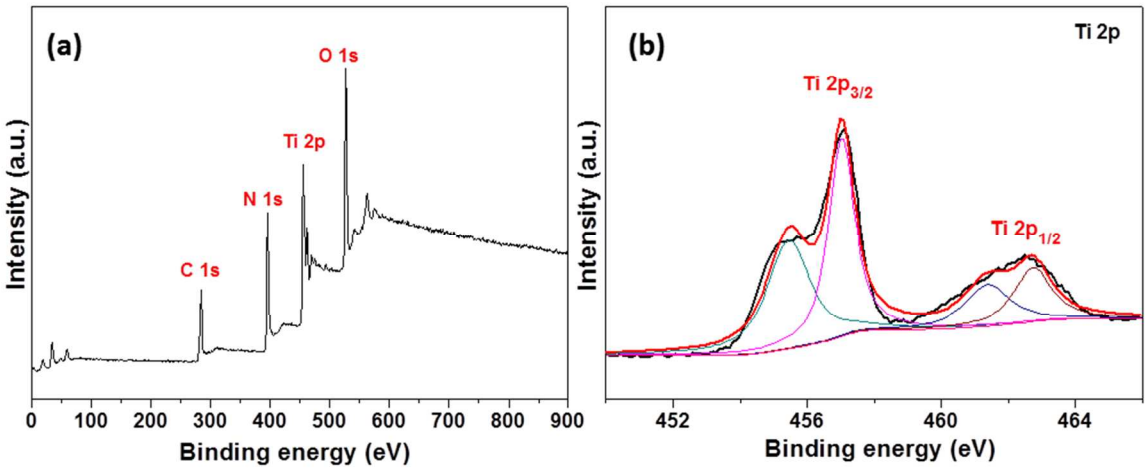

Fig. 4 (a) XPS survey scan of mpg-C_3N_4/TiO_2 heterojunctions and the corresponding Ti 2p high-resolution spectrum (b).

XPS measurement was carried out to obtain the information on oxidation state and surface chemical composition of the mpg-C_3N_4/TiO_2 heterojunctions sample. Survey spectra in Fig. 4a indicate the peaks of Ti, O, C, and N in the mpg-C_3N_4/TiO_2 composites. Fig. 4b shows high resolution spectra of Ti 2p transition. The Ti 2p peak is composed of spin doublets and the Ti 2p peak has two main components as determined by the fitting of the curve. The values of binding energies (BE) obtained for Ti $2p_{3/2}$ peak were 455.6 eV and 457.1 eV verify the Ti-N and intermediate phase, respectively.[36] Accordingly Ti $2p_{1/2}$ peaks were observed at 461.4 eV and 462.8 eV, respectively. The intermediate phase could be attributed to Ti_2O_3 or oxynitrides,[37] although their existence is still argued.[38, 39] The XPS results together with those from TEM and FTIR studies clearly reveal the formation of composite material with the chemically bound interfaces between mpg-C_3N_4 and TiO_2.

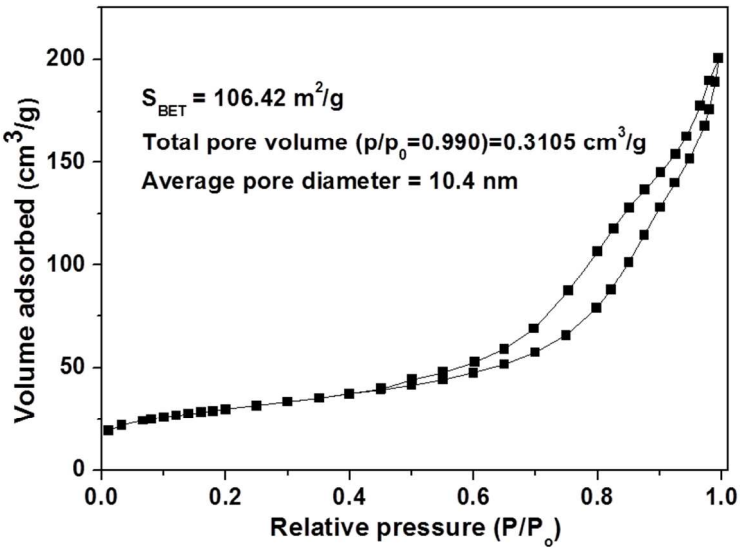

Fig. 5 N_2 adsorption-desorption isotherms of the as-prepared mpg-C_3N_4/TiO_2 heterojunctions.

In order to get more information on the porous structures, the as-prepared mpg-C_3N_4/TiO_2 heterojunctions sample was examined by N_2 sorption analysis. The N_2 adsorption-desorption isotherm of the sample is illustrated in Fig. 5. It can be observed that the mpg-C_3N_4/TiO_2 heterojunctions sample have type IV isotherm and type H3 hysteresis loop according to the IUPAC classification, which indicates mesoporous structures of the sample.[40] This is almost consistent with the TEM observation. Based on the desorption curve, the Brunauer-Emmett-Teller (BET) surface area of the porous mpg-C_3N_4/TiO_2 sample was calculated to be 106.42 m^2/g, a total pore volume was 0.3105 cm^3/g, and an average pore diameter was 10.4 nm.

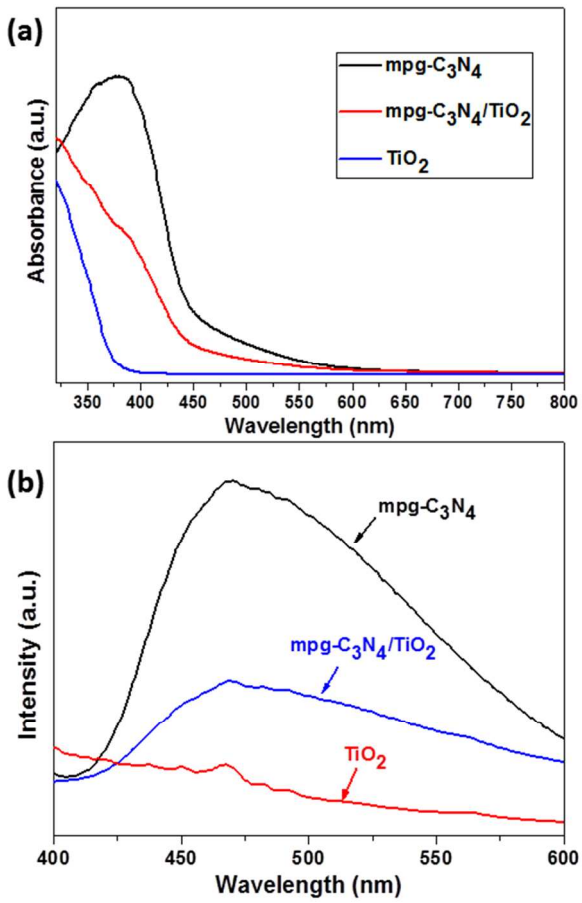

Fig. 6 Optical property of mpg-C_3N_4, TiO_2 and mpg-C_3N_4/TiO_2 heterojunctions. (a) UV-vis diffuse reflectance and (b) PL emission spectra monitored at an excitation wavelength of 325 nm.

Fig. 6a shows UV-vis diffuse reflectance spectra of the mpg-C_3N_4, TiO_2 and mpg-C_3N_4/TiO_2 heterojunctions samples. As a comparison, the absorption spectra of all the samples were carried out under the identical conditions. As illustrated in Fig. 6a, For pure TiO_2, the absorption occurs at wavelengths shorter than 390 nm, consistent with the intrinsic band gap of anatase TiO_2 (about 3.2 eV), while the absorption intensity of pure mpg-C_3N_4 rises rapidly at about 450 nm, in good accordance with the band gap of g-C_3N_4 (2.7 eV).[41] Compared with pure TiO_2, the mpg-C_3N_4/TiO_2 heterojunctions show additional absorption in the region of visible light, attributed to the existence of mpg-C_3N_4. Fig. 6b illustrates PL emission spectra of as-prepared samples monitored at an excitation wavelength of 325 nm. PL spectral analysis is applied to investigate the recombination rate of photogenerated electron-hole pairs. It was generally

believed that a lower PL emission intensity is an indication of a lower recombination of photogenerated electron-hole pairs. As can be seen, pure mpg-C_3N_4 has a strong peak around 460 nm in the PL spectrum, which can be attributed to the band-band PL phenomenon, i.e. the emission light energy is approximately equal to the bandgap energy of g-C_3N_4. Once TiO_2 nanoparticles were anchored on the mpg-C_3N_4 nanosheet, the emission intensity of PL spectra decreases significantly, suggesting that the mpg-C_3N_4/TiO_2 heterojunctions have a lower recombination rate of photo-generated electron-hole pairs than mpg-C_3N_4. This result shows good agreement with other heterojunction semiconductors.[22, 23]

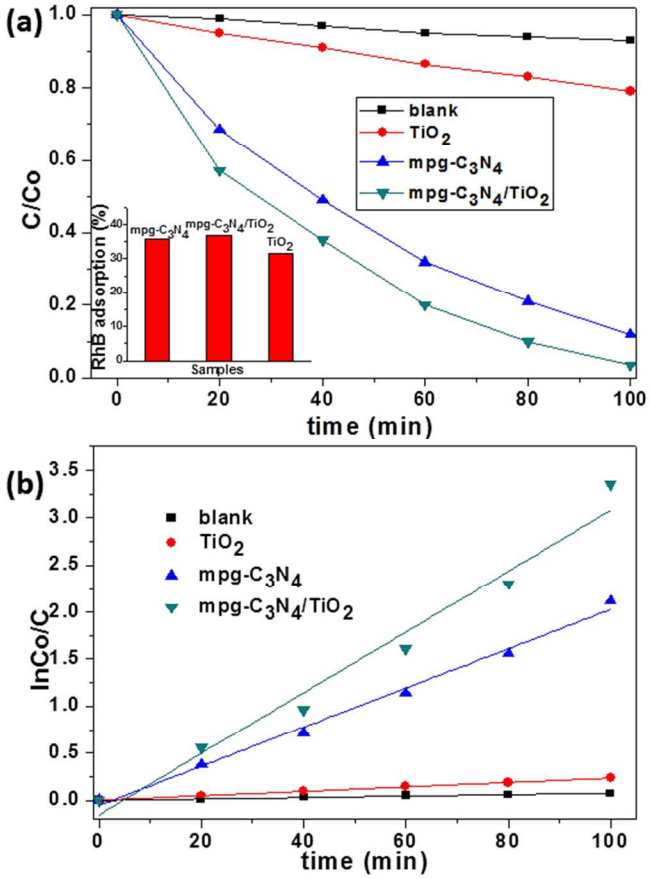

Fig. 7 Photocatalytic activities (a), adsorption capacities (inset) and kinetics (b) of the mpg-C_3N_4, TiO_2 and mpg-C_3N_4/TiO_2 heterojunctions for degradation of RhB under visible light irradiation.

Photocatalytic activity

Fig. 7a inset shows the RhB adsorption capacities of the samples, for the adsorption process

in the dark, the absorbance values of RhB decreased by 31.6%, 35.7% and 36.8%, due to absorption of RhB molecules by the TiO_2, mpg-C_3N_4 and mpg-C_3N_4/TiO_2 samples, respectively. The photocatalytic activity of the mpg-C_3N_4, TiO_2 and mpg-C_3N_4/TiO_2 heterojunctions were examined by visible-light degradation of RhB molecules in aqueous solution, where C is the concentration of RhB remaining in the solution after irradiation time t, and C_o is the initial concentration of RhB, and the results were shown in Fig. 7a. The blank experiment demonstrates that the decomposition of RhB is inappreciable within the test period in the absence of photocatalysts, suggesting that photolysis of RhB is negligible. As can be seen from Fig. 7a, the pure TiO_2 and mpg-C_3N_4 sample displayed a certain photocatalytic efficiency of 21% and 88% after visible-light irradiation for 100 min, respectively. As expected, the mpg-C_3N_4/TiO_2 heterojunctions exhibited higher photocatalytic activity than the pure mpg-C_3N_4 sample which provides 96.5% degradation of RhB under visible light irradiation. Fig. 7b reveals that the photocatalytic degradation of RhB on different catalysts fits pseudo-first-order kinetics, $\ln(C_o/C) = kt$, where C is the concentration of the RhB at time t, C_o is the initial concentration of the RhB solution, and the slope k is the apparent reaction rate constant. The results imply that k values for mpg-C_3N_4/TiO_2 sample is higher than those of pure mpg-C_3N_4 and TiO_2. It can be found that the k of mpg-C_3N_4/TiO_2 sample (0.0335 min^{-1}) is about 1.6 times that of mpg-C_3N_4 (0.0214 min^{-1}) and about 14 times that of TiO_2 (0.0024 min^{-1}). These results indicate that the formation of the heterojunction structure of mpg-C_3N_4/TiO_2 could greatly enhance the photocatalytic efficiency of single mpg-C_3N_4 and TiO_2. For evaluating the recyclability of the mpg-C_3N_4/TiO_2 sample, the additional experiments have been carried out to degrade RhB under visible light cycled for four times (Fig. 8). The photocatalytic activity of mpg-C_3N_4/TiO_2 heterojunctions sample for RhB degradation decreased from 96.5% to 88.5% after four cycling runs, which demonstrates that the mpg-C_3N_4/TiO_2 heterojunctions sample has high stability in the photocatalytic process under visible-light irradiation.

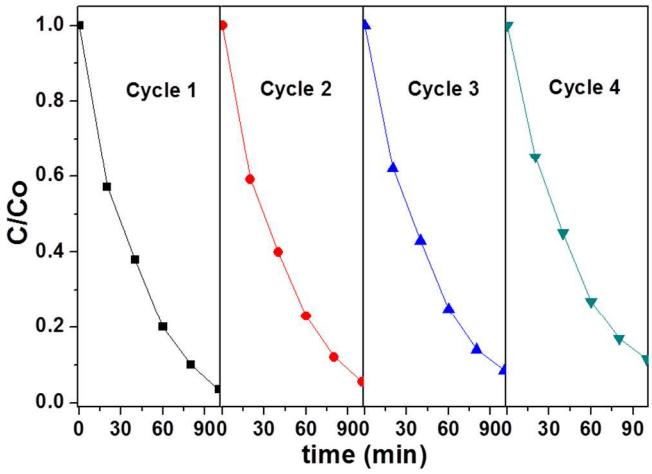

Fig. 8 Four photocatalytic degradation cycles of RhB by mpg-C_3N_4/TiO_2 heterojunctions under visible light irradiation.

Proposed mechanism for enhanced photocatalytic activity

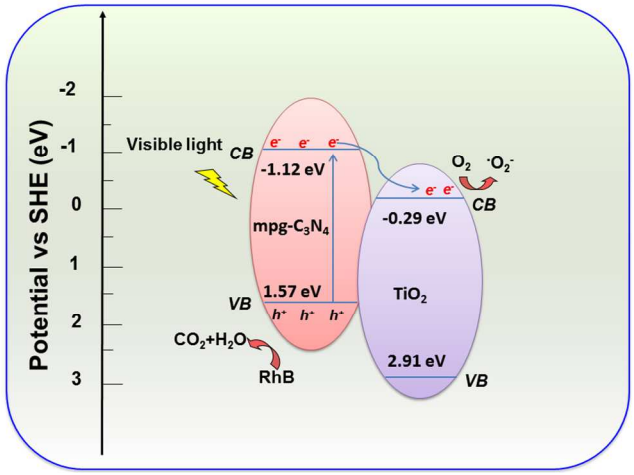

Fig. 9 Proposed photocatalytic mechanism for degradation of RhB over mpg-C_3N_4/TiO_2 heterojunctions under visible light irradiation.

On the basis of the above results and discussion, a photocatalytic mechanism for the under visible light irradiation is tentatively proposed and schematically illustrated in Fig. 9. When the as-prepared mpg-C_3N_4/TiO_2 heterojunctions are irradiated with visible light, the electrons get promoted from the valence band (VB) to the conduction band (CB) in mpg-C_3N_4, providing a route for electronic transition. According to previous studies, the CB and VB edge potentials of mpg-C_3N_4 were at -1.12 and 1.57 eV, respectively.[21] And the CB and VB edge potentials of TiO_2

were at -0.29 and 2.91 eV, respectively.[42] The CB edge potential of mpg-C_3N_4 is more negative than that of TiO_2 allowing the excited electron on the surface of mpg-C_3N_4 to transfer easily to TiO_2 via the well-built heterojunction. The recombination of photogenerated charge was inhibited and photocatalytic activities were enhanced effectively for TiO_2 which provides a site for electron translation. Then, the electrons stored in the CB of TiO_2 are trapped by the air near the surface of TiO_2 to form reactive $\bullet O_2^-$. Besides, the E_{VB} (g-C_3N_4, +1.57 eV vs SHE) values were lower than the standard redox potential of $\bullet OH/H_2O$ (+2.68 eV vs SHE), indicating that the photogenerated holes on mpg-C_3N_4 could not oxidize H_2O to active species •OH.[43, 44] Therefore, h^+ on the VB of mpg-C_3N_4 would react with RhB directly. On the other hand, as the electrons in CB of TiO_2 (−0.29 eV) located at more negative potential positions than the $O_2/\cdot O_2^-$ couple (−0.046 eV), electrons stored in the CB of TiO_2 are trapped by O_2 dissolved in the solution near the surface of TiO_2 to generate reactive superoxide radical ions ($\cdot O_2^-$), while the holes in the VB of mpg-C_3N_4 directly oxidize the pollutants.[45] Furthermore, the previously mentioned characterization indicates that coupling TiO_2 with mpg-C_3N_4 produces a well-contacted solid-solid heterojunction interface between mpg-C_3N_4 and TiO_2 semiconductor particles, which promotes the effective interfacial electron transfer and separation of photogenerated charge carriers, significantly enhancing photocatalytic activity.[46]

Conclusions

In summary, we have successfully fabricated mpg-C_3N_4/TiO_2 heterojunctions by using SiO_2 nanoparticles as hard template and cyanamide as precursor via a facile hard template approach. The obtained mpg-C_3N_4/TiO_2 heterojunctions exhibited enhanced photocatalytic activity toward RhB degradation under visible light irradiation than that of pure mpg-C_3N_4 and TiO_2 nanoparticles. This enhancement of the photocatalytic activity has been demonstrated due to the high separation and easy transfer of photogenerated electron-hole pairs at the heterojunction interfaces derived from the match energy level between the TiO_2 and mpg-C_3N_4. Thus, the mpg-C_3N_4/TiO_2 heterojunctions can

be a promising candidate for efficient visible light driven photocatalytic systems for organic pollution residues removal.

Acknowledgements

The authors are grateful to the financial supports of National Natural Science Foundation of China (Grant No. 21376051, 21306023, 21106017), Natural Science Foundation of Jiangsu (Grant No. BK20131288), Fund Project for Transformation of Scientific and Technological Achievements of Jiangsu Province of China (Grant No. BA2014100) and the Fundamental Research Funds for the Central Universities (3207045301, T15192014, KYLX_0161).

References

1. J. M. Hall-Spencer, R. Rodolfo-Metalpa, S. Martin, E. Ransome, M. Fine, S. M. Turner, S. J. Rowley, D. Tedesco and M.-C. Buia, *Nature*, 2008, **454**, 96-99.
2. M. A. Shannon, P. W. Bohn, M. Elimelech, J. G. Georgiadis, B. J. Mariñas and A. M. Mayes, *Nature*, 2008, **452**, 301-310.
3. C. J. Vörösmarty, P. McIntyre, M. O. Gessner, D. Dudgeon, A. Prusevich, P. Green, S. Glidden, S. E. Bunn, C. A. Sullivan and C. R. Liermann, *Nature*, 2010, **467**, 555-561.
4. M. R. Hoffmann, S. T. Martin, W. Choi and D. W. Bahnemann, *Chem. Rev.*, 1995, **95**, 69-96.
5. M. D. Hernandez-Alonso, F. Fresno, S. Suarez and J. M. Coronado, *Energ. Environ. Sci.*, 2009, **2**, 1231-1257.
6. V. Subramanian, E. Wolf and P. V. Kamat, *J. Phys. Chem. B*, 2001, **105**, 11439-11446.
7. L. Fan, J. Dongmei and M. Xueming, *J. Alloy. Compd.*, 2009, **470**, 375-378.
8. S.-Z. Chen, P.-Y. Zhang, D.-M. Zhuang and W.-P. Zhu, *Catal. Commun.*, 2004, **5**, 677-680.
9. F. Dong, W. Zhao and Z. Wu, *Nanotechnology*, 2008, **19**, 365607.
10. R. Jaiswal, N. Patel, D. Kothari and A. Miotello, *Appl. Catal. B: Environ.*, 2012, **126**,

47-54.

11. X. Cheng, X. Yu, Z. Xing and J. Wan, *Energy Procedia*, 2012, **16**, 598-605.
12. Z. Zhao, Y. Sun and F. Dong, *Nanoscale*, 2015, **7**, 15-37.
13. X. Wang, K. Maeda, X. Chen, K. Takanabe, K. Domen, Y. Hou, X. Fu and M. Antonietti, *J. Am. Chem. Soc.*, 2009, **131**, 1680-1681.
14. J. Yu, S. Wang, B. Cheng, Z. Lin and F. Huang, *Catal. Sci. Technol.*, 2013, **3**, 1782-1789.
15. K. Takanabe, K. Kamata, X. Wang, M. Antonietti, J. Kubota and K. Domen, *Phys. Chem. Chem. Phys.*, 2010, **12**, 13020-13025.
16. Z. Ding, X. Chen, M. Antonietti and X. Wang, *ChemSusChem*, 2011, **4**, 274-281.
17. Y. Di, X. Wang, A. Thomas and M. Antonietti, *Chemcatchem*, 2010, **2**, 834-838.
18. Y. Wang, R. Shi, J. Lin and Y. Zhu, *Energ. Environ. Sci.*, 2011, **4**, 2922-2929.
19. Y. Wang, X. Bai, C. Pan, J. He and Y. Zhu, *J. Mater. Chem.*, 2012, **22**, 11568-11573.
20. C. Pan, J. Xu, Y. Wang, D. Li and Y. Zhu, *Adv. Funct. Mater.*, 2012, **22**, 1518-1524.
21. X. Wang, K. Maeda, A. Thomas, K. Takanabe, G. Xin, J. M. Carlsson, K. Domen and M. Antonietti, *Nat. Mater.*, 2009, **8**, 76-80.
22. M. Xu, L. Han and S. Dong, *Acs Appl. Mater. Inter.*, 2013, **5**, 12533-12540.
23. D. Chen, K. Wang, T. Ren, H. Ding and Y. Zhu, *Dalton T.*, 2014, **43**, 13105-13114.
24. D. Jiang, L. Chen, J. Zhu, M. Chen, W. Shi and J. Xie, *Dalton T.*, 2013, **42**, 15726-15734.
25. J. Hong, S. Yin, Y. Pan, J. Han, T. Zhou and R. Xu, *Nanoscale*, 2014, **6**, 14984-14990.
26. J. Shen, H. Yang, Q. Shen, Y. Feng and Q. Cai, *Crystengcomm*, 2014, **16**, 1868-1872.
27. F. Goettmann, A. Fischer, M. Antonietti and A. Thomas, *Angew. Chem. Int. Edit.*, 2006, **45**, 4467-4471.
28. S. Yan, Z. Li and Z. Zou, *Langmuir*, 2010, **26**, 3894-3901.
29. X. Zhou, B. Jin, L. Li, F. Peng, H. Wang, H. Yu and Y. Fang, *J. Mater. Chem.*, 2012, **22**, 17900-17905.
30. B. Chai, T. Peng, J. Mao, K. Li and L. Zan, *Phys. Chem. Chem. Phys.*, 2012, **14**,

16745-16752.

31. Y. Yan, B. Hao, X. Wang and G. Chen, *Dalton T.*, 2013, **42**, 12179-12184.

32. F. Dong, L. Wu, Y. Sun, M. Fu, Z. Wu and S. Lee, *J. Mater. Chem.*, 2011, **21**, 15171-15174.

33. M. J. Bojdys, J. O. Müller, M. Antonietti and A. Thomas, *Chem. Eur. J.*, 2008, **14**, 8177-8182.

34. Y. Li, H. Zhang, P. Liu, D. Wang, Y. Li and H. Zhao, *Small*, 2013, **9**, 3336-3344.

35. C. Liu, D. Yang, Y. Jiao, Y. Tian, Y. Wang and Z. Jiang, *Acs Appl. Mater. Inter.*, 2013, **5**, 3824-3832.

36. A. Vesel, M. Mozetic, J. Kovac and A. Zalar, *Appl. Surf. Sci.*, 2006, **253**, 2941-2946.

37. J. Halbritter, H. Leiste, H. J. Mathes and P. Walk, *Fresen. J. Anal. Chem.*, 1991, **341**, 320-324.

38. H. C. Man, Z. D. Cui and X. J. Yang, *Appl. Surf. Sci.*, 2002, **199**, 293-302.

39. J. Kovac, G. Scarel, M. Sancrotti, M. G. Beghi, C. E. Bottani, P. M. Ossi, L. Calliari, M. Bonelli and A. Miotello, *J. Appl. Phys.*, 1999, **86**, 5566-5572.

40. K. S. Sing, *Pure Appl. Chem.*, 1985, **57**, 603-619.

41. Q. Sun, K. Lv, Z. Zhang, M. Li and B. Li, *Appl. Catal. B: Environ.*, 2015, **164**, 420-427.

42. S. Zhao, S. Chen, H. Yu and X. Quan, *Sep. Purif. Technol.*, 2012, **99**, 50-54.

43. L. Shi, L. Liang, J. Ma, F. Wang and J. Sun, *Catal. Sci. Technol.*, 2014, **4**, 758-765.

44. S. Kumar, T. Surendar, A. Baruah and V. Shanker, *J. Mater. Chem. A*, 2013, **1**, 5333-5340.

45. Y. F. Chen, W. X. Huang, D. L. He, S. T. Yue and H. Huang, *Acs Appl. Mater. Inter.*, 2014, **6**, 14405-14414.

46. K. Kondo, N. Murakami, C. Ye, T. Tsubota and T. Ohno, *Appl. Catal. B: Environ.*, 2013, **142**, 362-367.